Andrzej P. Nowak, Johan Hagberg*, Simon Leijonmarck, Hannah Schweinebarth, Darren Baker, Anders Uhlin, Per Tomani and Göran Lindbergh

# Lignin-based carbon fibers for renewable and multifunctional lithium-ion battery electrodes

https://doi.org/10.1515/hf-2017-0044
Received March 13, 2017; accepted August 15, 2017; previously published online September 13, 2017

**Abstract:** Lignin-based carbon fibers (LCFs) from the renewable resource softwood kraft lignin were synthesized via oxidative thermostabilization of pure melt-spun lignin and carbonization at different temperatures from 1000°C to 1700°C. The resulting LCFs were characterized by tensile testing, scanning electron microscopy (SEM), X-ray diffraction (XRD) and confocal Raman spectroscopy. The microstructure is mainly amorphous carbon with some nanocrystalline domains. The strength and stiffness are inversely proportional to the carbonization temperature, while the LCFs carbonized at 1000°C exhibit a strength of 628 MPa and a stiffness of 37 GPa. Furthermore, the application potential of LCFs was evaluated as negative electrodes in a lithium-ion battery (LIB) by electrochemical cycling at different current rates in a half-cell setup. The capacity drops with the carbonization temperature and the LCFs carbonized at 1000°C have a capacity of 335 mAh $g^{-1}$. All LCFs showed good cycling stability. Because of the mechanical integrity and conductivity of the LCFs, there is no need to apply current collectors, conductive additives or binders. The advantage is an increased gravimetric energy density compared to graphite, which is the most common negative electrode material. LCFs show a promising multifunctional behavior, including good mechanical integrity, conductivity and an ability to intercalate lithium for LIBs.

**Keywords:** lignin-based carbon fibers, lithium-ion battery, melt-spinning, multifunctional, softwood kraft lignin

***Corresponding author: Johan Hagberg,** Applied Electrochemistry, Department of Chemical Engineering, KTH Royal Institute of Technology, 100 44 Stockholm, Sweden, e-mail: johagb@kth.se. http://orcid.org/0000-0002-2029-4945
**Andrzej P. Nowak:** Applied Electrochemistry, Department of Chemical Engineering, KTH Royal Institute of Technology, 100 44 Stockholm, Sweden; and Faculty of Chemistry, Department of Chemistry and Technology of Functional Materials, Gdansk University of Technology, Narutowicza 11/12, 80-233 Gdansk, Poland
**Simon Leijonmarck:** Applied Electrochemistry, Department of Chemical Engineering, KTH Royal Institute of Technology, 100 44 Stockholm, Sweden; and Swerea KIMAB, Isafjordsgatan 28A, 164 40 Kista, Sweden
**Hannah Schweinebarth, Darren Baker, Anders Uhlin and Per Tomani:** Innventia AB, Drottning Kristinas väg 61, 114 28 Stockholm, Sweden
**Göran Lindbergh:** Applied Electrochemistry, Department of Chemical Engineering, KTH Royal Institute of Technology, 100 44 Stockholm, Sweden

## Introduction

Technical lignins are abundant, environmentally friendly and renewable carbon resources, which are available in large quantities as a byproduct of pulping. They are also effective precursors for carbon fiber (CF) manufacturing because of their low cost and high pyrolysis yields (Brodin et al. 2012). Currently, polyacrylonitrile (PAN) is the main precursor for CF production, and the cost of the least expensive final product is 21.7 USD $kg^{-1}$, which is high in comparison to the estimated lignin-based CFs (LCFs) (6.2 USD $kg^{-1}$), (Norberg 2012).

Lithium-ion batteries (LIBs) are an example of a rechargeable energy storage system, which are needed in portable electronic devices and electric vehicles. LIB production is considered to be a key technology towards electrification in many sectors and, thus, for moving away from the use of fossil fuels. In commercial LIBs, the negative electrode is made of synthetic or natural graphite due to its low cost, high specific capacity and excellent packing efficiency. The price of graphite in current battery applications is in the range of 5–20 USD $kg^{-1}$ (Focus Graphite Inc. 2016). New carbonaceous materials such as graphene, nanocarbons and nanofibers are expensive and non-renewable. Thus, renewable carbon resources are anticipated to replace graphite in LIBs. There are several carbonaceous materials originating from organic resources with promising capacities (Xing et al. 1996; Peled et al. 1998; Fey and Chen 2001; Fey et al. 2003; Stephan et al. 2006; Li et al. 2011), which, however, are expensive as alternative electrode materials in battery applications. LCFs have already been investigated as potential negative electrodes in LIBs in the form of fused electrospun CF mats (Wang et al. 2013), fused lignin mats (Tenhaeff et al. 2014) or as mixtures with amorphous carbon (Li et al. 2015). The precursors

tested varied between softwood (SW) and hardwood (HW) lignins, as well as mixtures with other materials. Other studies have demonstrated that lignin can also be used for positive electrodes, where the presence of the quinone group serves for electron and proton storage and exchange during redox cycling (Milczarek and Inganäs 2012) or as a binder material for LIBs (Lu et al. 2016). Furthermore, electrospun LCFs have been evaluated as electrodes in electric double-layer capacitors (You et al. 2015, 2016).

Advantages of using LCFs as LIB electrodes are the inherent conductivity and mechanical integrity, which eliminate the need for conductive additives, current collectors or binders. This is beneficial for the specific energy and energy density of the LIB. Another possible use for LCFs, due to the multifunctional nature of mechanical and electrochemical properties, is as electrodes in structural batteries, a battery that simultaneously holds a mechanical load (Liu et al. 2009).

The present study focuses on LCFs isolated from SW kraft lignin as a negative electrode material in LIBs. LCFs should be produced in the temperature range between 1000°C and 1700°C and the material characterized with differential thermal analysis (DTA), thermogravimetric analysis (TGA), mechanical tensile testing, scanning electron microscopy (SEM), X-ray diffraction (XRD) and confocal Raman spectroscopy.

## Materials and methods

**Preparation of LCFs:** Black liquor (BL) obtained from the industrial kraft pulping (Nordic Paper AS, Säffle, Sweden) of mixed pine and spruce was first separated by ultrafiltration [ceramic membrane: molecular weight cut-off (MWCO) 15 kDa] to recover a derivative permeate BL containing lignin of a lower molecular mass. The lignin was then isolated from the permeate BL according to the LignoBoost® procedure (Tomani 2010; Zhu et al. 2015) and dried in a vacuum oven at 80°C, and then heat-treated under vacuum at 200°C (2 h) to reduce volatile component content and to increase the glass transition temperature ($T_g$). The resulting lignin was extruded into lignin filaments by means of a multifilament melt-spinning unit and the filaments were converted to CFs. First, the filaments were mounted on a frame under tension and heated from 25°C to 120°C at 10°C $min^{-1}$, then to 240°C at 0.2°C $min^{-1}$, and finally to 250°C at a rate of 1.0°C $min^{-1}$. The filaments were then removed from the frame and carbonized at 1000, 1200, 1500 and 1700°C at a heating rate of 2.5°C $min^{-1}$ under nitrogen (for more details, see Supplementary Information).

**Lignin purity and thermal properties:** The experiments were performed in duplicate or triplicate via measuring the moisture content (MC), extractive content, carbohydrate content, Klason lignin content, acid-soluble lignin content, inorganic element content and ash content by standard analytical methods. The inorganic content of the lignin was characterized by optical emission spectroscopy.

The melt and softening behaviors of the lignin were characterized optically in a Fisher-Johns melting point apparatus (Thermo Fisher Scientific, Waltham, MA, USA). The $T_g$ was determined by DTA (Q1000 equipped with a RC90 cooling unit, TA Instruments, New Castle, DE, USA). TGA was performed (TA Instrument Q5000IR TGA) to assess the efficacy of the heat treatment (see Supplementary Information).

**Mechanical testing:** The data of the lignin and the carbonized LCF were evaluated by single filament tensile testing. The instruments used were a Dia-stron tensile testing system (LEX820) with an automatic sample loading system (ALS1500) and a laser dimension measurement system (LDS0200) for filament diameter determination (Dia-stron, Andover, Hampshire, UK). In brief, the filaments were carefully removed from the LCF bundles and mounted on tabs with an ultraviolet (UV)-active resin system. The tabs were held within a testing cartridge for multi-specimen testing; a sample test comprised a minimum of 24 successful specimen tests. The specimens had a gauge length of 20 mm; the strain rate was 0.1 mm $s^{-1}$. The displacement compliance of the system was found to be negligible and was within the range of 0.1%–0.25% of the gauge length of the specimen.

**Confocal Raman spectroscopy:** A HR800 UV Jobin Yvon Raman (Horiba, Kyoto, Japan) instrument in combination with a solid-state laser with a $\lambda_{max}$ excitation of 514 nm was used together with a 20× objective and a 600-groove $mm^{-1}$ density grating. Spectra were acquired over the range of 900–1900 $cm^{-1}$ with a resolution of 2 $cm^{-1}$. Depending on the signal intensity, up to three spectra were accumulated to obtain high signal/noise ratios with a total acquisition time of <2 min. The spectra were analyzed by two Lorentzian and two Gaussian peak-fitting models, and the $R^2$ values were found to be in the range of 0.9947–0.9969, indicating that the models for the four peaks were acceptable.

**XRD:** A Siemens diffractometer D5000 equipped with a Cu Kα/Kβ source was used. Each LCF sample was ground and placed in the sample holder of the instrument. A coupled scan was recorded, with diffraction angles between 10° and 70°, at a resolution of 0.04°; the duration of the test was 60 s.

**Electrochemical measurement:** The LCF samples were dried at 60°C under vacuum overnight prior to cell assembly to remove any potential water that would contaminate the electrolyte. A two-electrode pouch cell with LCF tows (around 200 fibers) was the working electrode, a copper foil connected to the ends of the LCF tow served as a current collector, a lithium foil was the counter/reference electrode, a 250-µm glass-microfiber filter (Whatman, GE Healthcare Life Sciences, Chicago, IL, USA) was the separator and the electrolyte was 1.0 M $LiPF_6$ in EC:DEC (1:1 w/w, LP40 Merck, Kenilworth, NJ, USA). Cell assembly was performed in a glove box in a dry argon atmosphere (<1 ppm $O_2$ and <1 ppm $H_2O$) at ambient temperature. The cell was tested under galvanostatic conditions in the potential range of 0.002–1.5 V vs. $Li/Li^+$ with a current density corresponding to 37.2 mA $g^{-1}$ (C/10 rate based on the theoretical maximum capacity of graphite, 372 mAh $g^{-1}$, and fully charged in 10 h). The electrical conductivity of a single LCF was measured according to the Kelvin method under constant current. All measurements were performed by means of a Gamry Series G 750 potentiostat (Gamry Instruments, Philadelphia, PA, USA).

# Results and discussion

## Lignin purity and thermal properties

The lignin data (Table 1) indicate a high purity (99.6%) with negligible carbohydrate, extractive and inorganic contents (see also Supplementary Information). The softening and melt behaviors of the lignin are presented in Table 2. Characteristics of the melting procedure were evaluated as softening and high flow behaviors, the first being the temperature at which the lignin appears to melt ($T_s$) and the second being the temperature at which the upper cover slip can be moved across the lower one ($T_{hf}$). $T_g$ data were measured by DTA, while TGA is indicative of the efficacy of the heat treatment (Figure 1). It is obvious that the heat treatment of the lignin was successful in eliminating potential volatiles, so that lignin could be melt-spun between 190°C and 210°C. Carbonization at 950°C gave a yield of 36.8% (see also Supplementary Information).

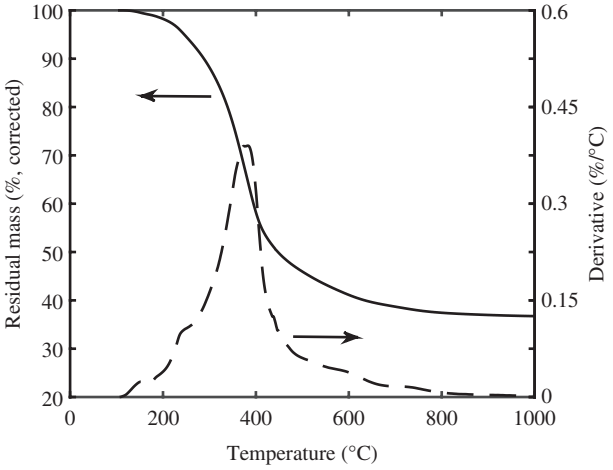


**Figure 1:** TGA data for the lignin, (-): residual mass (--): derivative.

## Mechanical properties of LCF

The tensile strengths and Young's moduli of the LCFs are presented in Table 3. With increasing carbonization temperature, the tensile properties decrease slightly in agreement with the literature data (Baker et al. 2010). The best mechanical performance is found for $LCF_{1000°C}$ with a tensile strength of 628 ± 106 MPa and a modulus of 37 ± 2 GPa. This is beneficial in terms of multifunctionality because this is the fiber with the highest reversible capacity (see following subsection). Compared to commercial PAN-based CFs, both the strength and modulus are almost an order of magnitude lower (Toray Carbon Fibers America, Inc., New York, NY, USA, 2016). The expectation is that there is a potential to improve the mechanical properties by optimizing the manufacturing methods. The LCF could, however, be considered for applications with lower demands on mechanical performance. It was described that the mechanical properties of LCFs are strongly affected by the precursor and the manufacturing process (Zhang and Ogale 2014a; Zhang et al. 2015). The tensile strengths and moduli of LCFs have been reported to be in the ranges of 150–1000 MPa and 28–83 GPa, respectively (Baker and Rials 2013; Zhang

**Table 3:** Tensile strengths and moduli of LCFs treated at different carbonization temperatures (Carb. T).

| Carb. T (°C) | Tensile strength (MPa) | Tensile modulus (GPa) |
|---|---|---|
| 1000 | 628 ± 106 | 37 ± 2 |
| 1200 | 585 ± 157 | 36 ± 2 |
| 1500 | 395 ± 112 | 31 ± 2 |
| 1700 | 363 ± 99 | 27 ± 2 |

**Table 1:** Lignin content and the amounts of different impurities.

| Lignin (mg $g^{-1}$) | | | Other materials (mg $g^{-1}$) | | | | | |
|---|---|---|---|---|---|---|---|---|
| Klason | Acid sol. | Total | CH[a] | Extr.[b] | Inorg.[c] | Total assay | Sulfur[d] | Lignin purity (%) |
| 896 | 102 | 998 | 2.2 | Trace | 1.9 | 1002 | 24.5 | 99.6 |

[a]Carbohydrates, [b]extractives, [c]inorganic elements (minus sulfur), [d]S assumed to be incorporated in lignin.

**Table 2:** Thermal properties of the lignin.

| DTA data | | | | Fisher-Johns | | TGA data | |
|---|---|---|---|---|---|---|---|
| $T_g$ (°C) | $T_{g\,(onset)}$ (°C) | $T_{g\,(offset)}$ (°C) | $\Delta C_p$ (J.(g.°C)$^{-1}$) | $T_s$ (°C) | $T_{hf}$ (°C) | $T_d$ (°C) | Mass at 950°C (%) |
| 128 | 122 | 133 | 0.51 | 165 | 173 | 382 | 36.8 |

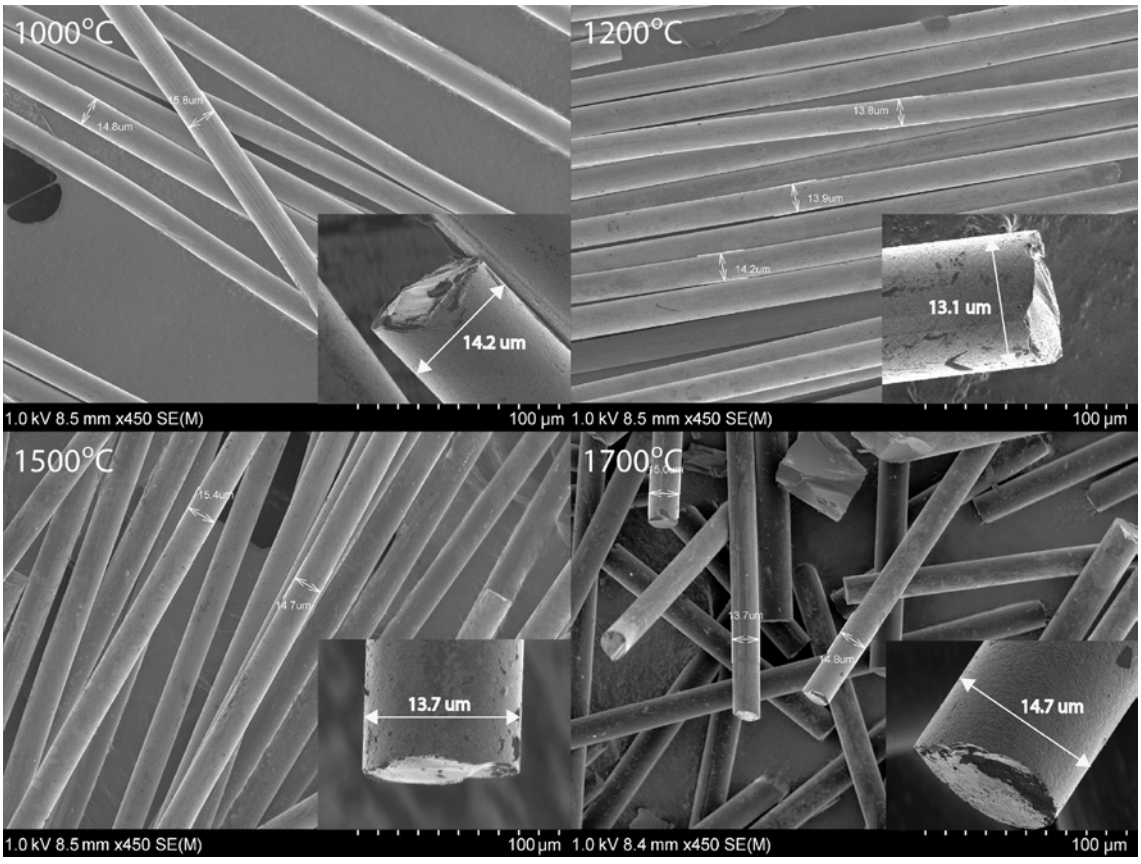


**Figure 2:** SEM images of LCF carbonized at temperatures of 1000, 1200, 1500, and 1700°C (from the upper left to the lower right). Magnification 450× (inset 5000×), accelerating voltage 1 kV.

and Ogale 2014b). This indicates that optimized lignins could have even better mechanical properties.

## SEM

The fiber diameters among LCFs vary between 13 µm and 15 µm (SEM images in Figure 2) and do not change significantly at different carbonization temperatures. The structure is macroscopically homogenous for all fibers, without obvious structural differences in the cross-section and thicknesses lengthwise. An exception is $LCF_{1000°C}$, where a thin shell around the fiber core was observed (see inset in Figure 2, top left). This could be due to different degrees of carbonization because of a lower temperature in the core, which seems to be of less importance at 1200°C and at temperatures >1200°C. Depending on the constituents in the shell, this could affect the electrochemical performance. A higher degree of graphitization with the graphite planes oriented along the surface could have a detrimental effect on rate performance because of blocking of lithium-ion pathways. The temperature is most likely too low to form any significant amount of crystalline graphite, so it is more probable that it is an effect of the amorphous carbon structure; in that case, the prediction concerning the electrochemical performance is difficult.

## Confocal Raman spectroscopy

Confocal Raman spectroscopy is well suited for the characterization of crystalline, nanocrystalline and amorphous carbonaceous materials (Tuinstra and Koenig 1970; Ferrari and Robertson 2000; Pimenta et al. 2007; Wilamowska et al. 2013; Nyczyk-Malinowska et al. 2014). The Raman spectra of LCFs are presented in Figure 3a, together with the spectrum of crystalline graphite for comparison. A common feature of the spectra is the maxima at ~1350 $cm^{-1}$ ("disordered" D band) and ~1600 $cm^{-1}$ ("ordered" G band), due to disordered and ordered graphite-like band lattices, respectively (Sadezky et al. 2005). The G band is due to $sp^2$ atoms in both rings and chains, while the D band is due to the breathing modes of $sp^2$ in rings only (Ferrari and Robertson 2004). The presence of disordered carbons is

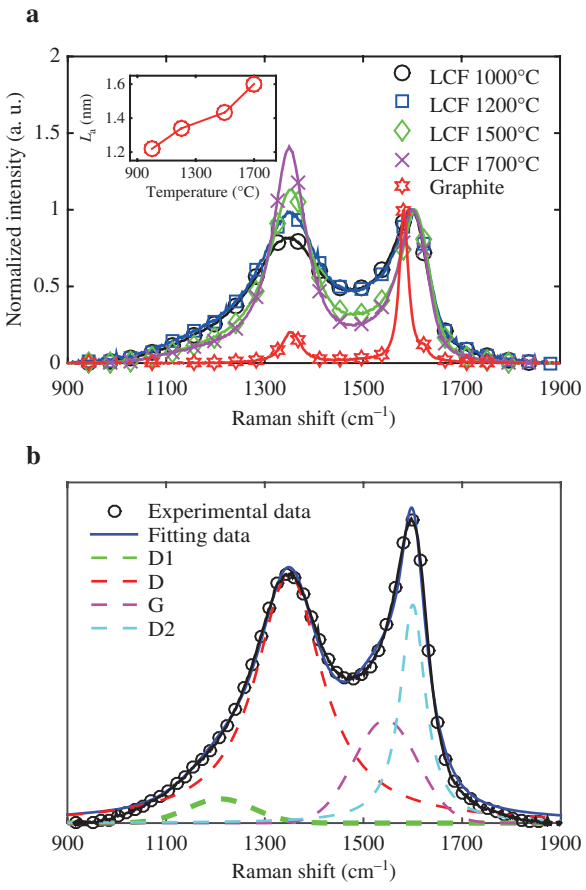


**Figure 3:** Raman spectra of LCFs.
(a) Raman spectra of LCFs carbonized at different temperatures and natural graphite for comparison. Inset: Cluster dimension ($L_a$) vs. carbonization temperature. (b) Curve fit for the first-order Raman spectra of LCFs annealed at 1000°C.

remarkable, though there is no graphitic ordering in the material (Ferrari and Robertson 2000).

With regard to amorphous carbon, it has been reported that it is as a superposition of four subbands (Sadezky et al. 2005). The Raman spectra of the LCFs were fitted with bands G, D, D1 and D2; for an explanation, see Table 4. An example of a curve fit is seen in Figure 3b.

Tuinstra and Koenig (1970) showed that the intensity of the D and the G bands depends on the type of carbonaceous material. The D band was attributed to a particle size of crystalline carbon domains known as in-plane correlation length or cluster size ($L_a$). Ferrari and Robertson (2000) proposed the following relationship for amorphous carbonaceous materials:

$$I(D)/I(G) = C'(\lambda) * L_a^2 \quad (1)$$

where $C'$ (514 nm) is equal to 0.0055 Å$^{-2}$ and $I(D)/I(G)$ is the intensity ratio between the D and the G bands. The

**Table 4:** First-order Raman bands and vibration modes (Sadezky et al. 2005).

| Band | Raman shift (cm$^{-1}$) | Vibration mode |
|---|---|---|
| G | ~1580 | In-plane, C-C stretch. ($E_{2g}$ symmetry) |
| D | ~1350 | In-plane, due to disorder ($A_{1g}$ symmetry) |
| D1 | ~1500 | Diamond-like, (sp$^3$ hybridized carbon) |
| D2 | ~1200 | In-plane, due to disorder or/and impurities ($A_{1g}$ symmetry) |

**Table 5:** Band position for curve-fitting first-order Raman spectra of LCFs carbonized at different temperatures.

| | Band (cm$^{-1}$) | | | | |
|---|---|---|---|---|---|
| Carb. T (°C) | D1 | D | D2 | G | $L_a$ (nm) |
| 1000 | 1210 | 1349 | 1545 | 1600 | 1.22 |
| 1200 | 1220 | 1354 | 1550 | 1604 | 1.34 |
| 1500 | 1215 | 1353 | 1542 | 1607 | 1.43 |
| 1700 | 1218 | 1350 | 1550 | 1603 | 1.60 |

considerable amount of amorphous carbon contained in the LCF mainly affects the band integrals but not the band intensities, which are only affected by the presence of six-fold aromatic rings (Ferrari and Robertson 2000). A summary of the Raman-derived data is presented in Table 5. The $L_a$ parameter slightly increases from 1.22 nm to 1.60 nm with carbonization temperature. Similar results were obtained for amorphous carbon (Cho et al. 1992; Wopenka and Pasteris 1993) and polycarbosilane-derived ceramics with the free carbon phase (Yan et al. 2010). The explanation is that the number of graphite nanocrystallites with few defects increases instead of the $L_a$ parameter increment. The grain size is considerably smaller than that of graphite (21.8 nm), which confirms an amorphous structure including only small crystalline inclusions. The carbonization temperature affects the short-range order, but $L_a$ is almost unchanged (Chu and Li 2006). Moreover, a temperature increase leads to a narrowing of the D and the G bands' full width at half maximum (FWHM), which confirms a higher crystalline order at a higher carbonization temperature.

## XRD measurements

XRD spectra for LCFs are presented in Figure 4. The 2θ peaks around 24° and 44° correspond to the graphitic 002 reflection and the 100 reflection, respectively. The interlayer spacing, $d_{002}$, was calculated under the Bragg

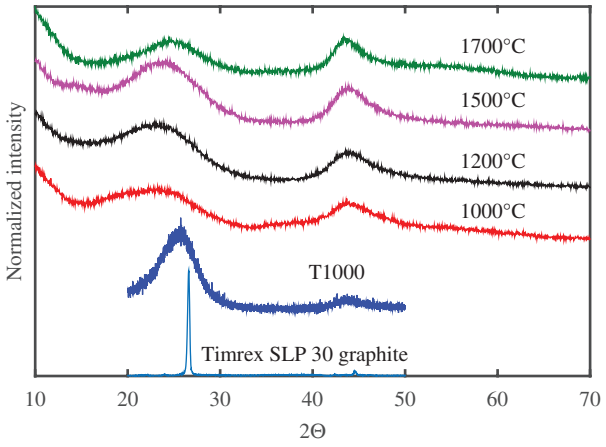


**Figure 4:** XRD spectra for LCF of different carbonization temperatures.
Timrex SLP 30 graphite and T1000 PAN-based carbon fiber data from a previous study (Hagberg et al. 2016). Intensity normalized for comparison.

condition. At 1000, 1200, 1500 and 1700°C, the interlayer spacing was 3.81, 3.76, 3.68 and 3.61 Å, respectively.

A graphite sample (Timrex SLP30) and a commercial PAN-based CF (T1000) were analyzed for comparison and the $d_{002}$ values were 3.35 Å and 3.49 Å, respectively. The much higher value of $d_{002}$ for the LCF indicates a low degree of crystallinity.

The average crystallite size, $L_c$, was calculated by the Scherrer formula with a shape factor of K = 0.934. This gives a lower boundary for the crystallite size as it is assumed that the entire peak broadening is due to crystallite size effects, though, in reality, defects and imperfections also give rise to peak broadening (Warren 1969). The $L_c$ values calculated from the 002 reflection are 1.07, 1.16, 1.27 and 1.32 nm at the carbonization temperatures of 1000, 1200, 1500, and 1700°C, respectively. The crystallite sizes for the Timrex SLP30 graphite and the T1000 CF were 39.5 nm and 2 nm, respectively. These results are consistent with the data of Tenhaeff et al. (2014). The crystallite sizes are very small (30 times smaller) than those of graphite, but they are only around two times smaller than in the case of commercial PAN-based CFs. Importantly, the large degree of defects and the amorphous carbon is problematic from an analytical point of view, and the actual crystallite sizes are most likely larger, but this analysis fairly approximates the crystallite sizes. With increasing carbonization temperatures, the interlayer spacing becomes smaller and the crystalline sizes larger. In other words, the degree of graphitization is increasing at higher temperatures, which is expected and also confirmed by the Raman spectroscopy. The carbonization temperatures are still too low to produce CFs with any significant graphite content.

## Electrical conductivity

The electrical conductivities of the LCFs carbonized at different carbonization temperatures before and after galvanostatic charging/discharging cycles are listed in Table 6. The electrical conductivity of LCFs increases with carbonization temperature. The difference of the data for $LCF_{1000°C}$ and $LCF_{1700°C}$ is, however, only 50 S cm$^{-1}$, i.e. the carbonization temperature does not have a large effect on the electrical properties. Moreover, the electrical conductivity of LCFs before and after galvanostatic charging/discharging is unchanged within the standard deviation (SD). Accordingly, the material maintains its electrical properties after cycling and the LCF is not damaged due to lithium intercalation/extraction. The conductivity values are over 10 times higher in comparison to the fused CFs in Wang et al. (2013), i.e. the LCF could be beneficial in terms of electrical properties in comparison with fused fibers. However, the conductivity of the LCF is still lower than that of commercially available PAN-based CFs, which is typically in the range of 588–1500 S cm$^{-1}$ (Toray Carbon Fibers America, Inc. 2016).

## Galvanostatic cycling

Three initial charging/discharging cycles of the LCF negative electrode materials at a current density equal to 37.2 mA g$^{-1}$ (nominal C/10 rate for graphite) are shown in Figure 5. In general, the first lithiation capacity is higher than in the following cycles. During the first cycle, lithium insertion into the carbonaceous materials forms a solid electrolyte interphase (SEI) due to reduction/oxidation reactions of solvents at the electrode surface (NuLi et al. 2006). Jacques et al. (2013) report about CFs that the first cycle capacity

**Table 6:** Electrical conductivity of LCFs before and after charging/discharging cycles.

| | Electrical conductivity (S cm$^{-1}$) | |
|---|---|---|
| Carb. T (°C) | Before | After |
| 1000 | 142 ± 14 | 139 ± 16 |
| 1200 | 146 ± 8 | 143 ± 33 |
| 1500 | 184 ± 24 | 180 ± 19 |
| 1700 | 191 ± 19 | 185 ± 4 |

The data are an average of three measurements with standard deviation (SD).

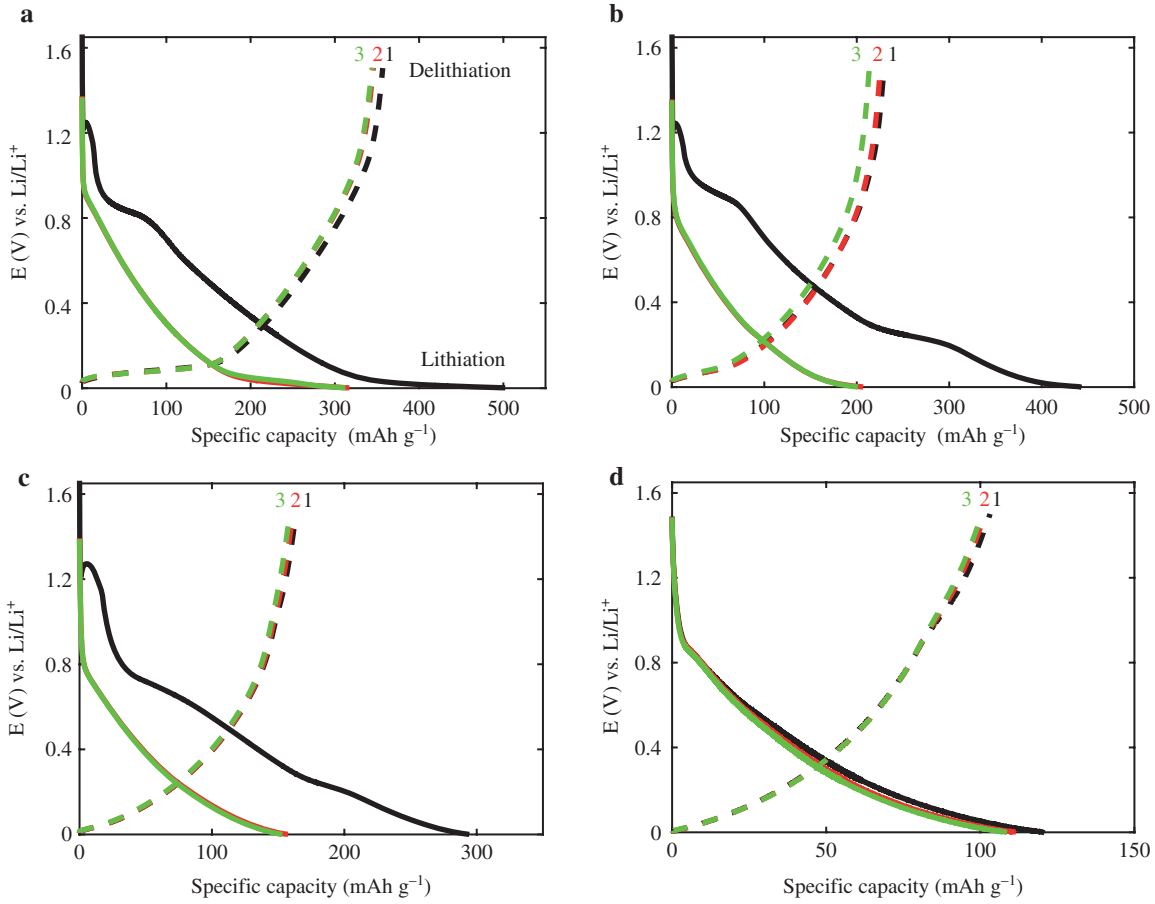


**Figure 5:** Voltage cycles of LCF.
The first three cycles of lithiation/delithiation into/from (a) LCF 1000°C, (b) LCF 1200°C, (c) LCF 1500°C and (d) LCF 1700°C negative electrode material at a C/10 rate.

drops (in addition to SEI formation) because lithium is trapped in the CF structure. Several mechanisms have been proposed regarding lithium insertion in disordered carbon materials in addition to the well-known intercalation between graphite planes: (1) insertion in microcavities, as small crystallites intersect randomly and form cavities able to store lithium (Dahn et al. 1995); (2) lithium bonding to hydrogen at edge sites of carbon layer planes for hydrogen-containing carbons (Dahn et al. 1995); (3) lithium bonding to carbon at edge sites and crystal surfaces associated with small crystallite sizes (Matsumura et al. 1995); and (4) covalently bonded $Li_2$ molecules (Sato et al. 1994). All of these processes and the presence of amorphous carbon and the turbostratic structure in the LCFs may affect the trapping process. This explains why the largest capacity drop is observed for the lowest carbonization temperature (with the highest amorphous carbon content) and decreases with temperature. A capacity drop was not observed in the first cycle of $LCF_{1700°C}$. This could partly be explained by a higher graphitization degree, although the disorder level is still significant. A lower capacity and, therefore, less inserted lithium could also be an explanation. Contrary to graphite (Kulova and Skundin 2006), the voltage profiles of the charging curves do not exhibit staging steps. This means that LCFs have no long-range crystalline order, similar to other types of CFs (Tenhaeff et al. 2014). The specific total discharge capacities for the LCF after the third cycle are 348, 215, 159 and 101 mAh $g^{-1}$ at carbonization temperatures of 1000, 1200, 1500 and 1700°C, respectively. Dahn et al. (1995) also observed this inverse relationship between capacity and carbonization temperature in the presence of disordered carbons.

The specific capacities of LCFs at different current rates and the coulombic efficiency (CE) are presented in Figure 6. The highest capacity is observed for a C/10 rate and diminishes with increasing current rate. However, it is noticeable that the LCF exhibits good cycling stability at different C rates. In all cases, when the current increases from C/10 to 1 C, the capacity drops to around half of the initial value. For $LCF_{1000°C}$, the capacity decreases further

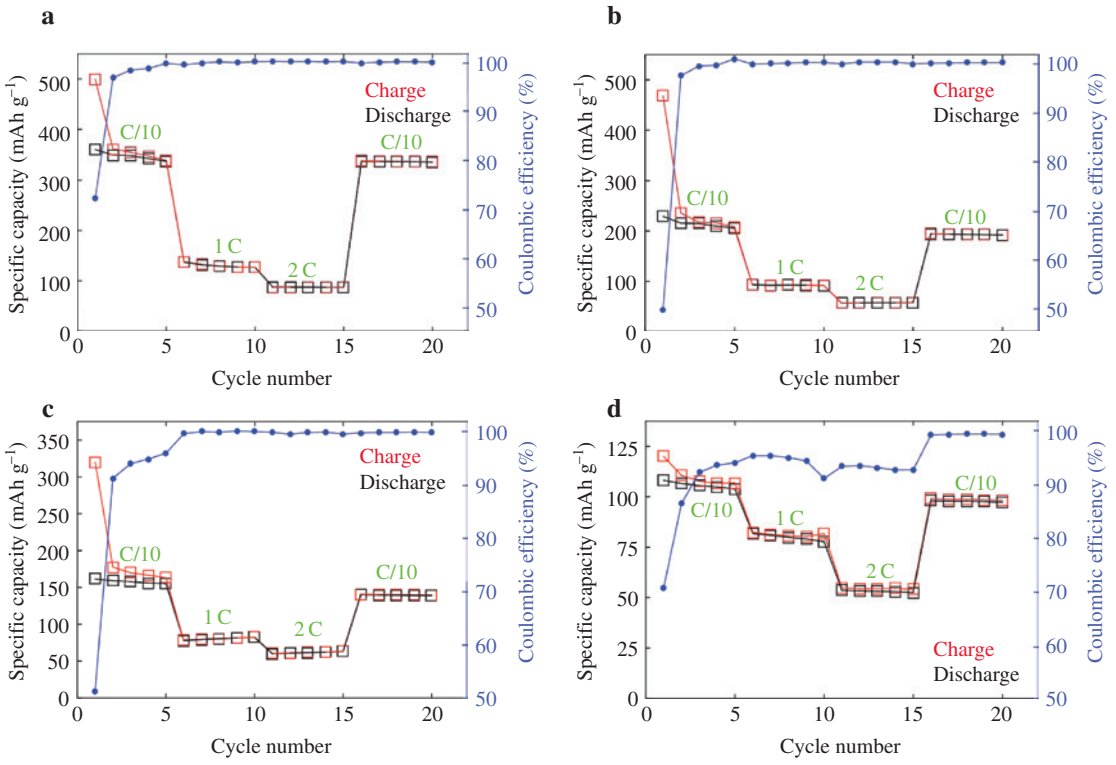


**Figure 6:** Rate performance of LCFs carbonized at different temperatures, (a) 1000°C, (b) 1200°C, (c) 1500°C, (d) 1700°C.

from ~130 mAh g$^{-1}$ at 1 C to 88 mAh g$^{-1}$ at 2 C. After five cycles at 2 C, low current (C/10) is applied again and the capacity increases to 335 mAh g$^{-1}$. It is noteworthy that the capacity retention for $LCF_{1000°C}$ is as high as 99.7% when a low current (C/10) is reapplied after five 1 C and five 2 C cycles. The capacity retention for the rest of the LCFs are 92, 89 and 94% at 1200, 1500 and 1700°C, respectively. The LCF negative electrodes still possess specific capacities close to the practical capacity of commercially available graphitic electrodes. As the LCFs simultaneously act as a current collectors and an active material, without any conductive additive or binder, the total weight of the electrode is lower than that of a traditional electrode design. Taking this into account, the specific capacity of the full electrode is even higher for $LCF_{1000°C}$ compared to a commercial graphite electrode combined with a metallic current collector. The specific capacities found in LCFs are similar to those reported in other recent studies (Wang et al. 2013; Tenhaeff et al. 2014). The average specific capacity of $LCF_{1000°C}$ is 335 mAh g$^{-1}$, and this is 4.2% lower in comparison to the LCF produced by Wang et al (2013) and 1.7 times greater than the LCF mats produced by Tenhaeff et al. (2014). The capacity of $LCF_{1000°C}$ is also on par with the data of other studies concerning commercial CFs produced for multifunctional use (Snyder et al. 2009; Kjell et al. 2011). Ultimately, it is demonstrated here that the origin of the lignin, the manufacturing process and the mode of electrode preparation have significant impacts on the final capacity of the electrodes. The first cycle drop is the largest issue for practical applications, and this has been observed previously for CFs with a significant degree of disorder (Hagberg et al. 2016). It could, however, be fixed with a pre-lithiation of the electrode, for instance. The initial CE varies between 50% and 70%, which is related to the large first cycle capacity drop. After a few cycles, the CE is increased to over 99%, which indicates a low amount of side reactions. The CE seems to decrease with carbonization temperature, probably because of a similar amount of SEI layer formation and side reactions for all electrodes, but the capacity is lower for a higher carbonization temperature, which leads to an apparent lower CE. The low CE, around 95%, for the first 15 cycles of $LCF_{1700°C}$ could be indicative of contaminations leading to side reactions.

## Full cell cycling

Cycling data from a full cell, consisting of an LCF negative electrode and a lithium iron phosphate (LFP) positive electrode is shown in Figure 7. The discharge capacity was found to be ~97 mAh g$^{-1}$ with a capacity retention of 97.8%

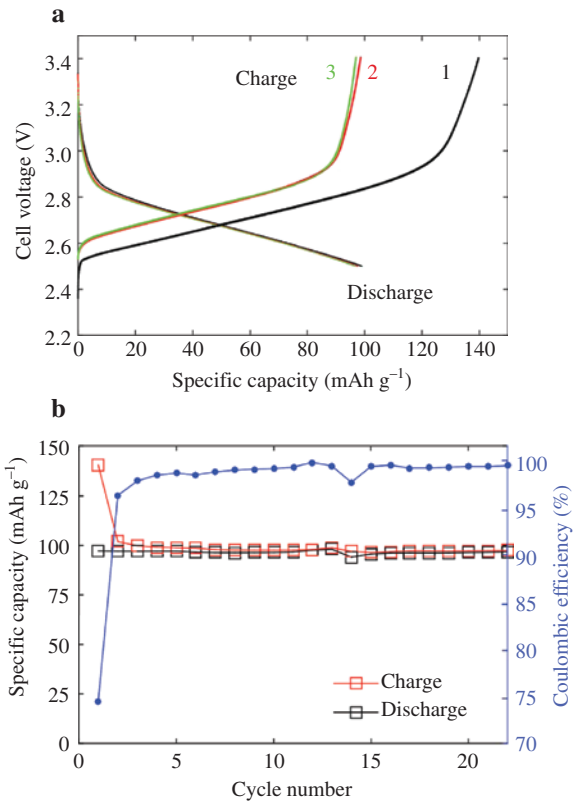


**Figure 7:** Voltage profiles (a) and extended cycling for full LCF/LiFePO4 cell (b).
(a) The charge/discharge curves of the LCF negative electrode with a commercial LiFePO4 positive electrode. The cell voltage varies between 2.5 V and 3.4 V, (b) extended cycling at C/10 rate.

after the third cycle. Extended cycling exhibited a CE of over 99%, with a capacity fading of 1.3% after 22 cycles. Four batteries of this type were constructed and tested, and they were able to fully supply a radio-controlled car (Innventia 2016). Thus, LCFs can be combined in a full battery pack to work as a negative electrode material in LIBs.

## Conclusions

The tensile strength and modulus are inversely dependent on carbonization temperature, and the best mechanical properties can be obtained for $LCF_{1000°C}$, giving rise to a material with a strength of 628 MPa and a modulus of 37 GPa. XRD and Raman measurements confirm a largely amorphous structure of the LCF, with some nanocrystalline domains, while the crystallite sizes were found to be only 1–2 nm. Increasing the carbonization temperature led to a slight decrease in disorder and an increased crystallinity. Galvanostatic cycling showed that the specific discharge capacity was highest for $LCF_{1000°C}$ (335 mAh $g^{-1}$). All LCFs exhibited good capacity retention after applying some cycles of higher currents and the cyclability was good. The first cycle drop is larger than for commercial LIB electrodes due to SEI layer formation and trapped lithium, which might limit practical applications. Pre-lithiating the fibers could be a possible remedy. The best candidate in terms of multifunctionality is $LCF_{1000°C}$, as this material has both the best mechanical properties and the highest specific capacity. The conductivity is sufficient at around 140 C $cm^{-1}$ and can be used without additional additives or current collectors, even if the conductivity is fairly high for LCFs carbonized at higher temperatures (around 190 C $cm^{-1}$ for $LCF_{1700°C}$). The expectation is not unrealistic that the mechanical properties can further be improved. The LCFs developed here are free-standing LCFs with inherent conductivity, mechanical integrity and high energy density, and can be produced at low costs.

**Acknowledgments:** Funding by The Swedish Energy Agency, project number 37712-1 “Structural Batteries for efficient vehicles”, is gratefully acknowledged. We acknowledge Birgitha Nyström from Swerea SICOMP for the preparation of LCFs in woven form.

## References

Baker, D.A., Rials, T.G. (2013) Recent advances in low-cost carbon fiber manufacture from lignin. J. Appl. Polym. Sci. 130:713–728.
Baker, F.S., Baker, D.A., Gallego, N.C. (2010) Proceeding. In SAMPE’10 Conference and Exhibition, Seattle, WA, May 17–20.
Brodin, I., Ernstsson, M., Gellerstedt, G., Sjöholm, E. (2012) Oxidative stabilisation of kraft lignin for carbon fibre production. Holzforschung 66:141–147.
Cho, N.H., Veirs, D.K., Ager, J.W., Rubin, M.D., Hopper, C.B., Bogy, D.B. (1992) Effects of substrate temperature on chemical structure of amorphous carbon films. J. Appl. Phys. 71:2243–2248.
Chu, P.K., Li, L. (2006) Characterization of amorphous and nanocrystalline carbon films. Mater. Chem. Phys. 96:253–277.
Dahn, J.R., Zheng, T., Liu, Y., Xue, J.S. (1995) Mechanisms for lithium insertion in carbonaceous materials. Science 270:590–593.
Ferrari, A.C., Robertson, J. (2000) Interpretation of Raman spectra of disordered and amorphous carbon. Phys. Rev. B 61:14095–14107.
Ferrari, A.C., Robertson, J. (2004) Raman spectroscopy of amorphous, nanostructured, diamond-like carbon, and nanodiamond. Philos. Trans. A. Math. Phys. Eng. Sci. 362:2477–2512.
Fey, G.T.K., Chen, C.L. (2001) High-capacity carbons for lithium-ion batteries prepared from rice husk. J. Power Sources 97–98: 47–51.
Fey, G.T.K., Lee, D.C., Lin, Y.Y., Prem Kumar, T. (2003) High-capacity disordered carbons derived from peanut shells as lithium-intercalating anode materials. Synth. Met. 139:71–80.

Focus Graphite Inc. Graphite 101 http://www.focusgraphite.com/technology/ (accessed Apr 20, 2016).

Hagberg, J., Leijonmarck, S., Lindbergh, G. (2016) High precision coulometry of commercial PAN-based carbon fibers as electrodes in structural batteries. J. Electrochem. Soc. 163:A1790–A1797.

Innventia, The fossil-free car of the future is in the forest, http://www.innventia.com/en/About-us/News1/The-fossil-free-car-of-the-future-is-in-the-forest/ (accessed Mar 16, 2016).

Jacques, E., Kjell, M.H., Zenkert, D., Lindbergh, G., Behm, M. (2013) Expansion of carbon fibres induced by lithium intercalation for structural electrode applications. Carbon N. Y. 59:246–254.

Kjell, M.H., Jacques, E., Zenkert, D., Behm, M., Lindbergh, G. (2011) PAN-based carbon fiber negative electrodes for structural lithium-ion batteries. J. Electrochem. Soc. 158:A1455.

Kulova, T.L., Skundin, A.M. (2006) Balance between reversible and irreversible processes during lithium intercalation in graphite. Russ. J. Electrochem. 42:251–258.

Li, W., Chen, M., Wang, C. (2011) Spherical hard carbon prepared from potato starch using as anode material for Li-ion batteries. Mater. Lett. 65:3368–3370.

Li, Y., Hu, Y.-S., Li, H., Chen, L., Huang, X.A. (2015) Superior low-cost amorphous carbon anode made from pitch and lignin for sodium-ion batteries. J. Mater. Chem. A 4:96–104.

Liu, P., Sherman, E., Jacobsen, A. (2009) Design and fabrication of multifunctional structural batteries. J. Power Sources 189:646–650.

Lu, H., Cornell, A., Alvarado, F., Behm, M., Leijonmarck, S., Li, J., Tomani, P., Lindbergh, G. (2016) Lignin as a binder material for eco-friendly Li-ion batteries. Materials (Basel) 9:1–17.

Matsumura, Y., Wang, S., Mondori, J. (1995) Interactions between disordered carbon and lithium in lithium ion rechargeable batteries. Carbon 33:1457–1462.

Milczarek, G., Inganäs, O. (2012) Renewable cathode materials from biopolymer/conjugated polymer interpenetrating networks. Science 335:1468–1471.

Norberg, I. Carbon fibres from kraft lignin, KTH Royal Institute of Technology, Stockholm, Sweden. 2002.

NuLi, Y., Yang, J., Jiang, Z. (2006) Intercalation of lithium ions into bulk and powder highly oriented pyrolytic graphite. J. Phys. Chem. Solids 67:882–886.

Nyczyk-Malinowska, A., Wójcik-Bania, M., Gumuła, T., Hasik, M., Cypryk, M., Olejniczak, Z. (2014) New precursors to SiCO ceramics derived from linear poly(vinylsiloxanes) of regular chain composition. J. Eur. Ceram. Soc. 34:889–902.

Peled, E., Eshkenazi, V., Rosenberg, Y. (1998) Study of lithium insertion in hard carbon made from cotton wool. J. Power Sources 76:153–158.

Pimenta, M., Dresselhaus, G., Dresselhaus, M.S., Cançado, L.G., Jorio, A., Saito, R. (2007) Studying disorder in graphite-based Systems by Raman spectroscopy. Phys. Chem. Chem. Phys. 9:1276–1291.

Sadezky, A., Muckenhuber, H., Grothe, H., Niessner, R., Pöschl, U. (2005) Raman microspectroscopy of soot and related carbonaceous materials: spectral analysis and structural information. Carbon N. Y. 43:1731–1742.

Sato, K., Noguchi, M., Demachi, A., Oki, N., Endo, M. (1994) A mechanism of lithium storage in disordered carbons. Science 264:556–558.

Snyder, J.F., Wong, E.L., Hubbard, C.W. (2009) Evaluation of commercially available carbon fibers, fabrics, and papers for potential use in multifunctional energy storage applications. J. Electrochem. Soc. 156:A215–A224.

Stephan, A.M., Kumar, T.P., Ramesh, R., Thomas, S., Jeong, S.K., Nahm, K.S. (2006) Pyrolitic carbon from biomass precursors as anode materials for lithium batteries. Mater. Sci. Eng. A 430:132–137.

Tenhaeff, W.E., Rios, O., More, K., McGuire, M.A. (2014) Highly robust lithium ion battery anodes from lignin: an abundant, renewable, and low-cost material. Adv. Funct. Mater. 24:86–94.

Tuinstra, F., Koenig J.L. (1970) Raman spectrum of graphite. J. Chem. Phys. 53:1126.

Tomani, P. (2010) The Lignoboost process. Cellul. Chem. Technol. 44:53–58.

Toray Carbon Fibers America, Inc. http://www.toraycfa.com/index.htm (accessed Apr 25, 2016).

Wang, S.X., Yang, L., Stubbs, L.P., Li, X., He, C. (2013) Lignin-derived fused electrospun carbon fibrous mats as high performance anode materials for lithium ion batteries. ACS Appl. Mater. Interfaces 5:12275–12282.

Warren, B.E. X-ray diffraction. Addison-Wesley Publishing Co., Boston, MA, USA. 1969.

Wilamowska, M., Graczyk-Zajac, M., Riedel, R. (2013) Composite materials based on polymer-derived SiCN ceramic and disordered hard carbons as anodes for lithium-ion batteries. J. Power Sources 244:80–86.

Wopenka, B., Pasteris, J.D. (1993) Structural characterization of kerogens to granulite-facies graphite: applicability of Raman microprobe spectroscopy. Am. Mineral. 78:533–557.

Xing, W., Xue, J.S., Zheng, T., Gibaud, A., Dahn, J.R. (1996) Correlation between lithium intercalation capacity and microstructure in hard carbons. J. Electrochem. Soc. 143:3482–3491.

Yan, M., Song, W., Zhao-Hui, C. (2010) Raman spectroscopy studies of the high-temperature evolution of the free carbon phase in polycarbosilane derived SiC ceramics. Ceram. Int. 36:2455–2459.

You, X., Koda, K., Yamada, T., Uraki, Y. (2015) Preparation of electrode for electric double layer capacitor from electrospun lignin fibers. Holzforschung 69:1097–1106.

You, X., Duan, J., Koda, K., Yamada, T., Uraki, Y. (2016) Preparation of electric double layer capacitors (EDLCs) from two types of electrospun lignin fibers. Holzforschung 70:661–671.

Zhang, M., Ogale, A.A. (2014a) Carbon fibers from dry-spinning of acetylated softwood kraft lignin. Carbon N. Y. 69:626–629.

Zhang, M., Ogale, A.A. (2014b) Carbon fibers from dry-spinning of acetylated softwood kraft lignin. In: Polymer Precursor-Derived Carbon, vol. 1173. Eds. Naskar, A.K., Hoffman, W.P. American Chemical Society, Washington. pp. 137–152.

Zhang, M., Jin, J., Ogale, A.A. (2015) Carbon fibers from UV-assisted stabilization of lignin-based precursors. Fibers 3:184–196.

Zhu, W., Westman, G., Theliander, H. (2015) The molecular properties and carbohydrate content of lignins precipitated from black liquor. Holzforschung 69:143–152.

**Supplemental Material:** The online version of this article offers supplementary material (https://doi.org/10.1515/hf-2017-0044).